Impedance scanning with chirps for single-phase converters

Sjur Føyen[1*], Chen Zhang[2], Marta Molinas[2], Olav Fosso[1] and Takanori Isobe[3]
1 Dept. of Electric Power Engineering, Norwegian University of Science and Technology, Trondheim, Norway
2 Key Laboratory of Control of Power Transmission and Conversion, Shanghai Jiao Tong Univerisity, Shanghai, China
3 Dept. of Engineering Cybernetics, Norwegian University of Science and Technology, Trondheim, Norway
4 Faculty of Pure and Applied Sciences, University of Tsukuba, Ibaraki, Japan
*E-mail: foyen.sjur@ntnu.no

***Abstract*—Impedance scanning of single-phase AC-DC converters is challenging due to frequency couplings, which map one injection frequency to a multiple of output frequencies. Single-tone injections are often preferred over wideband signals, as spectral overlap negates the benefits provided by quick-to-implement wideband scans. In this paper we take advantage of the time-frequency properties of chirp excitation signals, and develop a model so that a single chirp sweep can provide the impedance frequency response - formulated as a Harmonic Transfer Matrix, which takes into account the frequency couplings. Though we concentrate on single-phase AC-DC converters, the general HTM formulation extends application to any linear time-periodic and linear time-invariant system. Numerical impedance measurements are presented for a single-phase grid-connected converter, operating in grid-forming mode with dispatchable Virtual Oscillator Control.**

***Keywords*—Impedance scanning, chirp, Harmonic Transfer Function, dispatchable Virtual Oscillator Control**

I. Introduction

Numerous recent studies report the existence of frequency couplings in AC-DC converters, impacting tools and benchmarks for harmonic analysis, small-signal stability studies and control design. The issue is particularly notable in single-phase converters and asymmetric systems as they often contain more, and stronger, couplings. A general framework to handle couplings was formulated decades ago for helicopter rotor applications [1]. This framework is composed of the Harmonic Transfer Matrix (HTM) (following the convention in [2]) along with the Harmonic State Space (HSS), which are Linear Time-Periodic (LTP) equivalents of traditional transfer functions and state space models, respectively. In the early 2000s, the power electronics community started to realize the importance of periodic behaviour for stability assessment and subsequent control design [3][4]. More recent LTP analysis efforts have been directed towards single-phase Phase Locked Loops (PLLs) [5], Single Input Single Output (SISO) equivalents of grid-connected converters [6][7] and automated, parametric stability assessment [8].

The frequency coupling phenomena imposes a constraint on impedance scanning: there is no longer a one-to-one map between input and output frequencies. This is a major drawback for wideband excitation signals with subsequent spectral analysis, such as chirps, multitones, pseudorandom noise and binary sequences to mention a few. One must either tread carefully to avoid spectral overlap (see for example the sum of cosines [9]) or conduct as many linearly independent scans as there are couplings present in the system (see [10]). The consequence is that wideband impedance scanning takes much longer for an HTM than for a traditional transfer function. On the other hand, single-tone injections do not inflict spectral overlap (except at the harmonic frequencies), yet suffer from a trade-off between frequency resolution and number of injections [11]. In short, no existing method allows for swift and straight-forward impedance scanning. We bridge this gap by revisiting the chirp injection signal, and establish a time-frequency fitting procedure so that *a single* chirp signal enables HTM scans. The properties of a single chirp sweep are:

- Low measurement time
- Low requirements for injection equipment
- High-resolution frequency measurements
- Low crest factor
- The output is not in perfect steady-state

The first three points guarantee that early-stage scans are available at minimal effort - both for simulation and experimental studies. Low crest factor is a desirable wideband scan trait; the chirp exhibits low peak-to-average ratios which avoids excessive currents for a power electronics device under impedance scan with voltage injection. The last point hints to a reduction in accuracy. In section V we discuss this as a trade-off between accuracy and measurement time, limited by the poles of the system.

The notion of using chirps for frequency scanning is not new, in fact, chirps have a strong tradition in various fields - though mostly for LTI systems. As LTI transfer functions have a one-to-one map from input frequency to output frequency, Fourier based analysis like FFT or cross power spectral density methods can be directly applied. These approaches ignore the time dimension and care only for the spectral properties, and hence consider the chirp to be comparable to wideband signals that are only interpretable in frequency domain [12]. A recent technique originating from electrochemical applications, exploits the time-frequency property of the chirp by adopting an envelope-based approach [13]. Outputs containing multiple

chirps (which is precisely the case for HTMs) have much more complicated envelopes, hence that approach does not directly extend to HTM scanning. The method proposed in this paper is founded on a linear least-squares fit of a piecewise polynomial model onto the output response *in time domain*. The method provides (in addition to the properties of a single chirp excitation signal):

- Robustness to inconsistent sampling rates
- Inclusion of operating point in fit

The latter point allows scanning at the fundamental and harmonic frequencies, which is generally avoided (interpolated) for Fourier based methods. Quantitative comparisons with other wideband scanning techniques are subject to future endeavours. That will be important to reveal their performance in terms of accuracy. On this note, it is natural to mention that scanned impedances can fulfil several purposes - for instance 1) verification of an analytic HTM or HSS, 2) black-box impedance modelling with subsequent harmonic stability assessment and control design, and 3) vector-based fitting [11]. Any frequency domain impedance measurement approach should retain a level of accuracy as required by the subsequent analysis. Although extreme accuracy never hurts, it often entails equally extreme measurement efforts. For example, a comparison of accuracy for different truncations of analytic HTM impedance models as in [6], will require a very high accuracy for impedance verification scans. If the impedance is used to determine margins such as in [7], one may only care about accuracy in a specific frequency interval where the Nyquist curve is likely to reveal instability. In this paper we seek a simple and quick measurement technique which still provides relatively accurate scans.

The remainder of the paper is organised as follows: Section II presents a brief overview of impedance measurement in frequency coupled (LTP) systems. Section III lays out the piecewise polynomial chirp response model along with a few important extensions. Section IV provides numerical results and comparisons with the analytic model. Section V addresses unresolved issues, and Section VI wraps up the findings in some concluding remarks.

II. Harmonic Transfer Matrix (HTM) scanning

A. HTM Notation

In the HTM equation $\mathbf{\Delta y(s)} = \mathbf{H(s)\Delta u(s)}$, $\mathbf{H(s)} \in \mathbb{C}^{(2N+1)\times(2N+1)}$ denotes the HTM from a small signal input $\mathbf{\Delta u(s)} \in \mathbb{C}^{(2N+1)\times 1}$ to a small signal output $\mathbf{\Delta y(s)} \in \mathbb{C}^{(2N+1)\times 1}$ where N is by definition infinity but usually set to a low number encompassing the dominant couplings (truncation). $\mathbf{H}$ generally has the structure in (1), given a fundamental frequency ω_f. An element of the HTM $\mathbf{H}$, H_n, is called a Harmonic Transfer Function (HTF), following the convention in [2].

$$\mathbf{H} = \begin{bmatrix} \ddots & \vdots & \vdots & \vdots & \iddots \\ \dots & H_0(s-j\omega_f) & H_{-1}(s) & H_{-2}(s+j\omega_f) & \dots \\ \dots & H_{+1}(s-j\omega_f) & H_0(s) & H_{-1}(s+j\omega_f) & \dots \\ \dots & H_{+2}(s-j\omega_f) & H_{+1}(s) & H_0(s+j\omega_f) & \dots \\ \iddots & \vdots & \vdots & \vdots & \ddots \end{bmatrix} \tag{1}$$

B. Single tone perturbation

For a single perturbation frequency ω_p in Δu, the ouput Δy is determined by the middle column of $\mathbf{H}$

$$\begin{bmatrix} \vdots \\ \Delta y(j[\omega_p - \omega_f]) \\ \Delta y(j\omega_p) \\ \Delta y(j[\omega_p + \omega_f]) \\ \vdots \end{bmatrix} = \begin{bmatrix} \vdots \\ H_{-1}(j\omega_p) \\ H_0(j\omega_p) \\ H_{+1}(j\omega_p) \\ \vdots \end{bmatrix} \Delta u(j\omega_p) \tag{2}$$

Note that (2) only holds if the input harmonics can be controlled individually so that the input contains one and only one frequency, which is in general not possible in presence of feedback. In such cases it might be better to measure the SISO-equivalent [6].

From (2), the ideal output as would stem from the steady-state response to a single sine input with amplitude A_{in} and frequency ω_p, pertains to (3).

$$\Delta y(t) = A_{in} \sum_{n=-N}^{N} A_n sin((\omega_p + n\omega_f)t + \theta_n) \tag{3}$$

with $A_n = |H_n(j(\omega_p)|$ and $\theta_n = \angle H_n(j(\omega_p)$ which are the absolute value and phase of the Harmonic Transfer Functions (HTFs), respectively, that we want to identify. Hence, the single-tone approach is as simple as they come: inject *one* sine, wait for the transient to dissipate, measure the output, and compute the impedance through FFT or cross power spectral density.

The perk of this approach is that it fits very well with the mathematical model, and thus provides extremely accurate results. Still, high resolution requires proportionally many perturbations - which yields large measurement time to capture higher order transfer functions. Another issue is that spectral overlap occurs if the system is perturbed at a harmonic frequency, which is more a practical concern rather than a limitation; a resonance centered at a harmonic frequency can be captured by perturbing not exactly at the harmonic frequency, but around it.

C. Chirp perturbation

Define the chirp input perturbation as:

$$\begin{aligned} \Delta u(t) &= A_{in} sin(\phi(t)) \\ &= A_{in} sin(\int \omega(t) dt) \end{aligned} \tag{4}$$

where - if the chirp is linear - $\omega(t) = \omega_0 + 2\pi kt$ with k as the linear chirp rate. In this paper we opt for the linear chirp

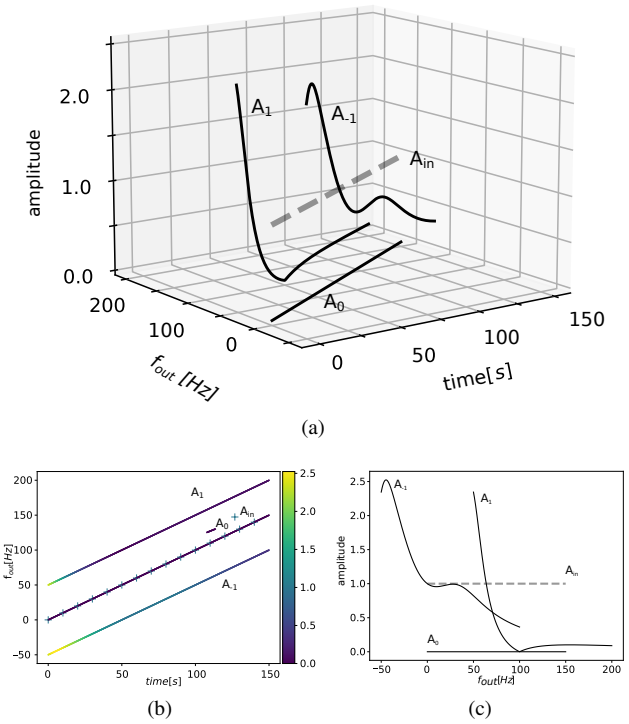

(a)

(b)

(c)

Fig. 1. Chirp outputs for a SOGI-PLL HTM: (a) 3-d plot depicting the amplitudes of (5) as functions of time and frequency (b) projection onto the time-frequency plane, with heat bar added to depict the amplitudes (c) projection onto the frequency-amplitude plane

as it is easy to visualize and straightforward to implement. Still, other types of phase functions ($\phi(t)$'s) should eventually form part of the chirp excitation signal repertoire.

The chirp sweep relies on the assumption that the output pertains to (3) for a time-varying frequency, that is,

$$\Delta y(t) = A_{in} \sum_{n=-N}^{N} A_n(t) sin(\phi_n(t) + \theta_n(t)) \tag{5}$$

with $A_n(t) = |H_n(j(\omega(t))|$, $\phi_n(t) = \phi(t) + n\omega_f$ and $\theta_n(t) = \angle H_n(j(\omega(t))$.

A discussion on this assumption can be found in section V.

As illustration, a frequency-fixed SOGI-PLL with $k_{sogi} = 4$ and bandwidth $\alpha_{pll} = 200$Hz is perturbed with a linear chirp with rate $k = 1$. Its HTM describes the linearised relationship between voltage as input and phase as output. The phase output contains multiple chirps, which ideally should have amplitudes described by the elements of the middle column of this HTM. These chirp amplitudes are plotted in Fig 1a, and only two are nonzero - A_{-1} and A_1 - a frequency adaptive SOGI-PLL will typically have a few more nonzero HTFs (see [14] for HTM modelling of SOGI-based synchronisation), and in the general case there will be $2N + 1$ HTFs to consider. The chirp outputs are well separated in the time-frequency domain as can be seen in Fig 1b, yet overlap if the temporal location is ignored, as seen from the projection of the HTFs onto the frequency-amplitude axes in Fig. 1c.

III. Polynomial HTF chirp response

To decompose $\Delta y(t)$ into its different harmonic components, we opt for a polynomial model of the HTFs. First, we reformulate (3) so that the HTFs are represented by their real and imaginary parts $\alpha_n(t) = Re\{H_n(j\omega(t))\}$ and $\beta_n(t) = Im\{H_n(j\omega(t))\}$, respectively.

$$\Delta y(t) = A_{in} \sum_{n=-N}^{N} [sin(\phi_n(t))\alpha_n(t) + cos(\phi_n(t))\beta_n(t)] \tag{6}$$

Setting a polynomial model for α_n and β_n of order P as in (7) yields (8).

$$\begin{aligned} \alpha_n(t) &= \sum_{p=0}^{P} \alpha_{n,p} t^p \\ \beta_n(t) &= \sum_{p=0}^{P} \beta_{n,p} t^p \end{aligned} \tag{7}$$

$$\Delta y(t) = A_{in} \sum_{n=-N}^{N} \sum_{p=0}^{P} [sin(\phi_n(t))t^p \alpha_{n,p} + cos(\phi_n(t))t^p \beta_{n,p}] \tag{8}$$

A discussion of the polynomial order follows in section V.

In (8), the only unknown values are the polynomial coefficients $\alpha_{n,p}$'s and $\beta_{n,p}$'s. This permits formulation of a linear least squares regression problem, on matrix form as

$$\underbrace{\begin{bmatrix} \Delta y(t_0) \\ \Delta y(t_1) \\ \vdots \\ \Delta y(T) \end{bmatrix}}_{\mathbf{\Delta y}} = \underbrace{\begin{bmatrix} \overrightarrow{r_{-N}}(t_0) & \dots & \overrightarrow{r_N}(t_0) & \overrightarrow{q_{-N}}(t_0) & \dots & \overrightarrow{q_N}(t_0) \\ \overrightarrow{r_{-N}}(t_1) & \dots & \overrightarrow{r_N}(t_1) & \overrightarrow{q_{-N}}(t_1) & \dots & \overrightarrow{q_N}(t_1) \\ \vdots & \ddots & \vdots & \vdots & \ddots & \vdots \\ \overrightarrow{r_{-N}}(T) & \dots & \overrightarrow{r_N}(T) & \overrightarrow{q_{-N}}(T) & \dots & \overrightarrow{q_N}(T) \end{bmatrix}}_{\mathbf{C}} \underbrace{\begin{bmatrix} \overrightarrow{\alpha_{-N}} \\ \vdots \\ \overrightarrow{\alpha_N} \\ \overrightarrow{\beta_{-N}} \\ \vdots \\ \overrightarrow{\beta_N} \end{bmatrix}}_{\mathbf{x}} \tag{9}$$

where

$$\begin{aligned} \overrightarrow{r_n}(t) &= [sin(\phi_n(t)), sin(\phi_n(t))t^1, ..., sin(\phi_n(t))t^P] \\ \overrightarrow{q_n}(t) &= [cos(\phi_n(t)), cos(\phi_n(t))t^1, ..., cos(\phi_n(t))t^P] \\ \overrightarrow{\alpha_n} &= [\alpha_{0,n}, \alpha_{1,n}, ..., \alpha_{P,n}]^\intercal, \overrightarrow{\beta_n} = [\beta_{0,n}, \beta_{1,n}, ..., \beta_{P,n}]^\intercal \end{aligned}$$

With N_T as the number of samples, the matrix $\mathbf{C}$ is of size N_T by $P * 2(2N + 1)$. Once (9) is solved - in the least squares sense - for the polynomial coefficients, all $\alpha_n(t)$ and $\beta_n(t)$ can be recovered with (7). The amplitude and phase of the n'th HTF can subsequently be calculated as

$$A_n(t) = \sqrt{\alpha_n(t)^2 + \beta_n(t)^2} \tag{10}$$

$$\theta_n(t) = tan^{-1}(\frac{\beta_n(t)}{\alpha_n(t)}) \tag{11}$$

In principle, a high degree polynomial could fit the frequency response of any transfer function with poles in the left half plane. Yet, higher order polynomials drastically increase

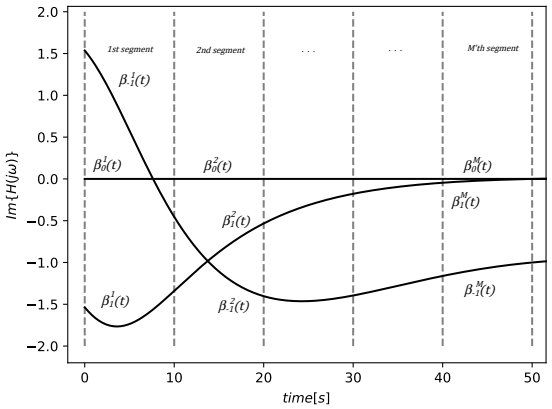

Fig. 2. Piecewise modelling of the HTFs, for the same SOGI-PLL as in Fig 1a - the real part, α, follows the same pattern.

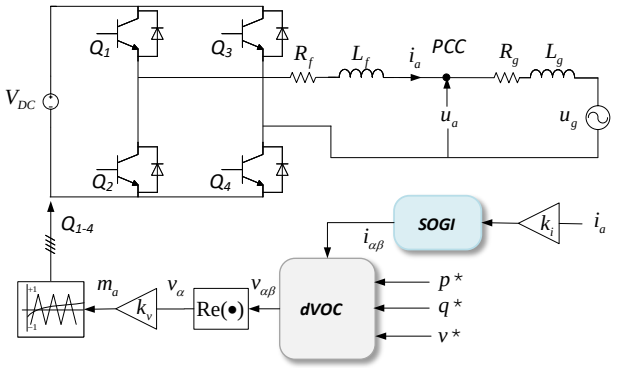

Fig. 3. Single-phase converter connected to a grid, in grid forming mode with dispatchable virtual oscillator control

the chances of overfitting - an issue that is further exacerbated by having multiple HTF outputs *and* periodic steady-states in a single time-domain measurement. In the following we present two important extensions to (9): 1) inclusion of an operating point, and 2) piecewise polynomial HTFs.

A. Inclusion of an operating point

As in some practical cases it can be challenging to discard a periodically varying operating point (i.e., discern the small signal response from the measured response), the operating point should simply be incorporated in (3). Without either removing the operating point or including it in the model, underfitting is likely to occur which renders the results useless.

In the case of the operating point containing only a fundamental component, (6) is extended with a single component with ϕ_n calculated from the fundamental frequency and $k = 0$. This component should usually be of constant amplitude and phase and hence can be modelled with $P = 1$.

B. Piecewise polynomial HTFs

Polynomial splines provide inspiration for a piecewise polynomial model to address the overfitting issue: divide the HTF into low order polynomial segments (splines), and apply boundary conditions to tie them together (knots). The new splines problem is implemented by duplicating (9) for M segments, as illustrated (for β only) in Fig. 2, yielding (12).

$$\begin{bmatrix} \mathbf{\Delta y_0} \\ \mathbf{\Delta y_1} \\ \mathbf{\Delta y_2} \\ \vdots \\ \mathbf{\Delta y}_M \end{bmatrix} = \begin{bmatrix} \mathbf{C_0} & 0 & 0 & \dots & 0 \\ 0 & \mathbf{C_1} & 0 & \dots & 0 \\ 0 & 0 & \mathbf{C_2} & \dots & 0 \\ \vdots & \vdots & \vdots & \ddots & \vdots \\ 0 & 0 & 0 & \dots & \mathbf{C}_M \end{bmatrix} \begin{bmatrix} \mathbf{x_0} \\ \mathbf{x_1} \\ \mathbf{x_2} \\ \vdots \\ \mathbf{x}_M \end{bmatrix} \tag{12}$$

Then, define the boundary conditions at each knot. These can be placed on the α and β values directly as in (13), and on their derivatives - for $m = 1$ to $m = M - 1$.

$$\begin{aligned} \alpha_{n,m}(T) &= \alpha_{n,m+1}(t_0) \\ \beta_{n,m}(T) &= \beta_{n,m+1}(t_0) \end{aligned} \tag{13}$$

In vector form,

$$\begin{aligned} [1, T, ..., T^P]\overrightarrow{\alpha_{n,m}} &= [1, t_0, , ..., t_0^P]\overrightarrow{\alpha_{n,m+1}} \\ [1, T, ..., T^P]\overrightarrow{\beta_{n,m}} &= [1, t_0, , ..., t_0^P]\overrightarrow{\beta_{n,m+1}} \end{aligned} \tag{14}$$

The boundary conditions add $2N(M-1)$ rows to (12); the equations in (14) must be inserted at their corresponding indices. Finally the polynomial HTMs with boundary conditions can be solved with a weighted linear least-squares fit. Some empirical thumb-rules for weight selection are: 1) Boundary conditions for the AC operating point should be strong (i.e., have high weights), 2) boundary conditions for derivatives should be weak if the number of segments are high. 3) Around resonances it is usually better to choose many segments with weak boundary conditions than high polynomial orders and strong boundary conditions.

IV. Simulation results

With purpose of demonstration, a single-phase VSC connected to an ideal grid is simulated in PSCAD/EMTDC, in grid forming mode with dispatchable Virtual Oscillator Control (dVOC) as first presented in [15] and experimentally verified in [16]. As this is a single-phase system, dVOC requires the use of an Orthogonal System Generator (OSG) to generate a suitable $\alpha\beta$-vector for the current. The Second Order Generalized Integrator (SOGI) is a potential candidate for this role. The converter parameters are listed in Table I.

The middle HTM column is found in three ways: 1) Chirp scanning, 2) single-tone scanning and 3) analytic modelling. The analytic model is found by setting up the state-space equations (which are included in the appendix), and applying the Automatic Model Generation (AMG) as presented in [17]. The HSS is transformed to HTM for u_a as input and $-i_a$ as output, which is interpreted as the output admittance of the converter. Furthermore, eigenanalysis on the HSS gives the weakest pole (in the fundamental strip [1]) at approximately $s = -21.3 \pm 26.5j$, the low damping caused by interactions between the SOGI, dVOC and L-filter.

The impedance scanning and HSS modelling are both conducted in pu values, on bases corresponding to the converter

TABLE I
CONVERTER PARAMETERS

Ratings					
S_b	1 kVA	V_b	126 V (rms)	ω_f	100π rad/s
Circuit parameters (pu)					
$X_f(\omega_f)$	0.1	R_f	0.01	$\lvert u_g \rvert$	0.95
Control parameters					
k_i	0.089 A^{-1}	k_v	178 V	f_{sw}	10 kHz
η	5	μ	10	k_{sogi}	3
Setpoints (in pu.)					
$p*$	1.0	$q*$	0.44	v^*	1.0

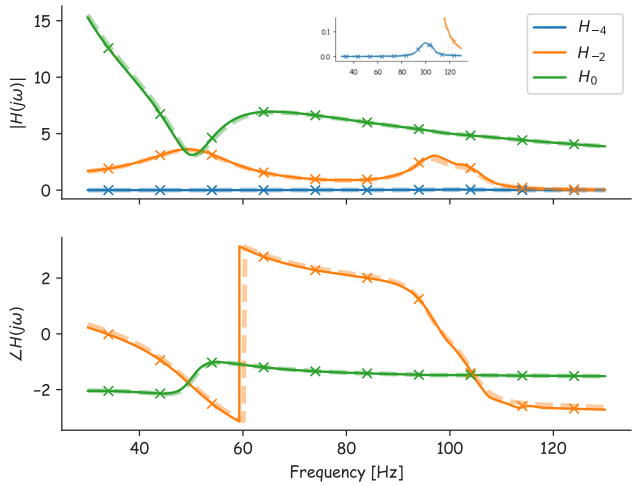

Fig. 4. Amplitude and phase of the converter admittance obtained by chirp scanning (solid line), analytic modelling (dashed line) and single-tone scanning (cross markers)

ratings. The setpoints are consistent with the power flow solution, and current and voltage scalings (k_i and k_v) are chosen so that all oscillator values have unity amplitude at rated conditions. The injection is implemented as a series voltage perturbation at the PCC, and the grid impedance is set to zero.

A linear chirp with $k = 5$, starting at 20 Hz is applied for 22 seconds, ending at 130Hz. In this frequency range, the couplings due to control are strongest - particularly around 50Hz and 100Hz. The first two seconds are discarded to exclude the initial transient, then processed by the polynomial chirp decomposition in (12), with 50 segments and N = 4. A similar procedure is conducted for the single-tones: 10 tones are injected one by one, separated by 10Hz, for 2 seconds. The first second is discarded and FFT is applied to the remaining second. Alias issues are avoided in both cases by passing the output current through a 3rd order butterworth filter with 1500Hz bandwidth, the filter gain and phase lag are compensated *after* computing the transfer function response. Only the HTFs with $max(|H(j\omega|) > 0.01$ are plotted in Fig 4, the phase of H_{-4} is omitted as its amplitude is very low. The chirp, single tone and analytic model agree very well, albeit with a negligible discrepancy between the analytic model and the scans. The HTM should be particularly hard to identify at $\omega_p = \omega_f$, as three signals are mixed at 50Hz in the output: the operating point, and the 0 and -2 couplings. In time-frequency domain this is not a problem, as these harmonics are distinguishable before and after $\omega_p = 2\pi 50 rad/s$. Continuity of the HTFs through the piecewise polynomial model ensures that their frequency response at the fundamental is captured as well.

V. DISCUSSION

A. Error of chirp excitation compared to single-tones

The transfer function frequency response to an arbitrarily fast chirp compared to that of a pure tone, is hard to define analytically. The deviation is largest around the poles, both real and complex. If the chirp sweeps past a weak pole too quick, not only will it fail to capture the transfer function around the pole frequency but also at frequencies after that; the pole is excited and the free response dissipates slowly due to low damping. This phenomena can be avoided altogether by ensuring

$$k \leq \frac{\sigma^2}{2\pi} |\varepsilon_r|_{max} \tag{15}$$

around a pole with real part σ, with maximum relative deviation of the transfer function $|\varepsilon_r|_{max} << 1$ (see appendix for derivation). That is easily achieved if the system is well damped - if not, it will significantly increase the measurement time by requiring an excessively low chirp rate. Eq. (15) hints towards straightforward solutions to improve the chirp speed vs. accuracy trade-off - for example by adopting varying chirp rate, with slow rate around the weak poles and higher rate elsewhere. Still, eq. (15) is conservative and does not mean the chirp rate cannot be faster around the weak poles - merely that it would lead to deviation from steady-state which have yet to be quantified. The weakest pole for the dVOC in section IV gives $k < 7.2$ for $|\varepsilon_r|_{max} < 0.1$, and $k = 5$ conforms to that. Now, the dVOC is retuned with $k_{sogi} = 4$, shifting the weakest pole in the fundamental strip to $s = -9.1 \pm j16.4$. Eq. (15) yields $k < 1.3$, and Fig. 5 shows that the admittance is inaccurate around the resonance of H_{-2} at approximately 100Hz.

B. Polynomial order and number of segments

Without any *a priori* knowledge of the poles, one cannot provide rigorous thumb-rules for selection of the polynomial order and number of segments. While higher polynomial orders in theory are able to fit high order transfer functions with weak poles, they dramatically increase the risk of overfitting. Nonetheless, if (15) holds, the fit is relatively robust to the choice of segments and polynomial order. Second to fourth order polynomials and many segments usually yield a good fit.

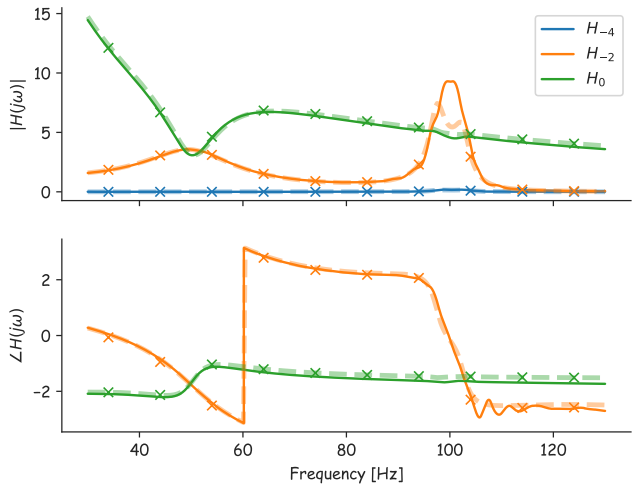

Fig. 5. Admittance of dVOC with $k_{sogi} = 4$. The chirp sweeps past the resonance too fast, yielding a bad fit.

C. Computational complexity

Solving the linear least squares problem is the most computationally expensive task by far in the piecewise polynomial HTF fit, of complexity $\mathcal{O}(N_T(NPM)^2)$. High harmonic order N to account for the general case, combined with many number of segments M *and* highly oversampled data is a recipe for hours of waiting. The results presented in Fig 4 ($N = 4$, $P = 3$, $M = 50$, $N_T = 10000$) take around 16 seconds to process, in a Python implementation on a high-end laptop. We expect future improvements such as faster chirps (reduce N_T), smart segment selection (reduce M) and dominant coupling detection (reduce N) to bring processing time down to a fraction of this. As an example - for the same case as in Figure 4 but with $M = 25$ and ignoring odd couplings, the processing time is approx. 1 second, albeit with a slight decrease of accuracy around 100 Hz.

VI. Conclusion

This paper has presented a chirp impedance scanning procedure for frequency coupled systems - which in general cannot be scanned by a single wideband signal *if* the output is analysed purely in frequency domain. The chirp bypasses this limitation if analysed in time-frequency domain. Thus, *one* chirp can provide the frequency scan of the Harmonic Transfer Matrix impedance or admittance representation. The analysis is based on a piecewise polynomial model of the Harmonic Transfer Functions and a linear least squares fit, which presents a variety of combinations of segmentation and polynomial order. If the chirp is designed according to the weakest pole in the system, the post-processing is shown to be robust. We only give a conservative boundary for the chirp rate, and there might be considerable potential in faster chirps. PSCAD simulations and Python post-processing demonstrate the scanning procedure on a dispatchable Virtual Oscillator Control operated single-phase Voltage Source Converter.

VII. Acknowledgements

The authors would like to acknowledge the open access publication support to the project "NTNU-Chinese Collaboration on Next Generation Power Electronics Converters for Renewable Energy (CoNeCt)" 309253 funded by the Research Council of Norway under the INTPART programme.

Appendix

A. VSC State space model

$$\text{dVOC}\begin{cases} \dot{v_\alpha} = -\omega_f v_\beta + \eta(\mu\phi v_\alpha + \dfrac{v_\alpha q^* - v_\beta p^*}{v^{*2}} + x_\beta) \\ \dot{v_\beta} = \omega_f v_\alpha + \eta(\mu\phi v_\beta + \dfrac{v_\alpha p^* + v_\beta q^*}{v^{*2}} - x_\alpha) \end{cases}$$

$$\text{SOGI}\begin{cases} \dot{x_\alpha} = k_{sogi}(i_a - x_\alpha\omega_f - x_\beta\omega_f) \\ \dot{x_\beta} = x_\alpha\omega_0 \end{cases}$$

$$\text{Circuit}\begin{cases} \dot{i_a} = \frac{1}{L}(v_\alpha - Ri_a - u_a) \end{cases}$$

B. Chirp error at a weak pole

Given a s-domain transfer function with a weakly damped resonance at ω_r

$$H(s) = \frac{1}{s^2 + 2\sigma s + \omega_r^2} \tag{16}$$

and its time-domain differential equation, excited with a complex exponential chirp signal at arbitrary starting frequency ω_0 and phase θ_0

$$\ddot{y} + 2\sigma\dot{y} + \omega_r^2 y = e^{j(\theta_0 + \omega_0 t + \varphi(t))} \tag{17}$$

with $\varphi(t) = k\pi t^2$ for a linear chirp. An explicit solution for the response $y(t)$ is not feasible - however, it is possible to obtain an approximate solution through a MacLaurin series expansion of $e^{j\varphi(t)}$.

$$u(t) \approx e^{j(\theta_0 + \omega_0 t)}(1 + j\pi k t^2) \tag{18}$$

The first term in (18) induces the ideal forced response to a constant frequency complex exponential input. The second term will be used to quantify the chirp error, i.e., $y_{forced}(t) = y_{ideal}(t) + \varepsilon(t)$.

$$\ddot{\varepsilon} + 2\sigma\dot{\varepsilon} + \omega_r^2\varepsilon = j\pi k t^2 e^{j(\theta_0 + \omega_0 t)} \tag{19}$$

Guess the solution of $\varepsilon(t)$

$$\varepsilon(t) = e^{j(\theta_0 + \omega_0 t)}[At^2 + Bt + C] \tag{20}$$

Insert (20) in (19) and collect the power terms on each side. Solve for A, then B and finally C.

$$\begin{aligned} A &= jk\pi H(j\omega_0) \\ B &= -j4\pi k[j\omega_0 + \sigma]H(j\omega_0)^2 \\ C &= j8\pi k[j\omega_0 + \sigma]^2 H(j\omega_0)^3 + j\pi k H(j\omega_0)^2 \end{aligned}$$

Since the series expansion contains an arbitrary starting frequency ω_0 and phase θ_0, $\varepsilon(t)$ can be evaluated at $t = 0$.

$$\varepsilon = Ce^{j\theta_0} \tag{21}$$

More interesting is the relative error ε_r

$$\varepsilon_r = \frac{\varepsilon}{H(j\omega_0)} \tag{22}$$

which amplitude has its maximum at $\omega_0 \approx \omega_r$

$$|\varepsilon_r|_{max} \approx \frac{2\pi k}{\sigma^2} \tag{23}$$

Therefore, setting k as in (15) ensures the error is bounded by $|\varepsilon_r|_{max}$.

For a real (negative) pole

$$H(s) = \frac{1}{s+\sigma} \tag{24}$$

the same procedure yields

$$\dot{y} + \sigma y = e^{j(\theta_0+\omega_0 t)}(1 - j2\pi k t^2) \tag{25}$$

$$\begin{aligned} A &= jk\pi H(j\omega_0) \\ B &= -j2\pi k H(j\omega_0)^2 \\ C &= j2\pi k H(j\omega_0)^3 \end{aligned}$$

$$\varepsilon_r(t) = j2\pi k H(j\omega)^2 e^{j(\theta_0+\omega_0 t)} \tag{26}$$

which has its maximum at $\omega_0 = 0$

$$|\varepsilon_r|_{max} = \frac{2\pi k}{\sigma^2} \tag{27}$$

This is identical to the second order system chirp error in (23).

REFERENCES

[1] N. M. Wereley, "Analysis and control of linear periodically time varying system," Ph.D. dissertation, Massachusetts Inst. Technol., 1991.

[2] P. Vanassche, G. Gielen, and W. Sansen, *Systematic Modeling and Analysis of Telecom Frontends and Their Building Blocks*, 1st ed., ser. The Springer International Series in Engineering and Computer. New York, NY: Springer-Verlag, 2005, vol. 842.

[3] E. Mollerstedt and B. Bernhardsson, "Out of control because of harmonics-an analysis of the harmonic response of an inverter locomotive," *IEEE control systems*, vol. 20, no. 4, pp. 70–81, 2000.

[4] J. Rico, M. Madrigal, and E. Acha, "Dynamic harmonic evolution using the extended harmonic domain," *IEEE Transactions on Power Delivery*, vol. 18, no. 2, pp. 587–594, 2003.

[5] S. Golestan, J. M. Guerrero, J. Vasquez, A. Abusorrah, and Y. Al-Turki, "Standard sogi-fll and its close variants: Precise modeling in ltp framework and determining stability region/robustness metrics," *IEEE Transactions on Power Electronics*, vol. 36, no. 1, pp. 409–422, 2021.

[6] C. Zhang, M. Molinas, S. Føyen, J. Suul, and T. Isobe, "Harmonic-domain siso equivalent impedance modeling and stability analysis of a single-phase grid-connected vsc," *IEEE Transactions on Power Electronics*, vol. 35, no. 9, pp. 9770–9783, 2020.

[7] Q. Qian, S. Xie, J. Xu, K. Xu, S. Bian, and N. Zhong, "Output impedance modeling of single-phase grid-tied inverters with capturing the frequency-coupling effect of pll," *IEEE Transactions on Power Electronics*, vol. 35, no. 5, pp. 5479–5495, 2020.

[8] C. Zhang, T. Isobe, J. Suul, T. Dragicevic, and M. Molinas, "Parametric stability assessment of single-phase grid-tied vscs using peak and average dc voltage control," *IEEE Transactions on Industrial Electronics*, pp. 1–1, 2021.

[9] E. K. Hidir, I. Uyanik, and O. Morgül, "Harmonic transfer functions based controllers for linear time-periodic systems," *Transactions of the Institute of Measurement and Control*, vol. 41, no. 8, pp. 2171–2184, 2019.

[10] E. Siddiqi, "Identification of the harmonic transfer functions of a helicopter rotor," Master's thesis, Massachusetts Inst. Technol., 1999.

[11] V. Salis, A. Costabeber, S. M. Cox, F. Tardelli, and P. Zanchetta, "Experimental validation of harmonic impedance measurement and ltp nyquist criterion for stability analysis in power converter networks," *IEEE Transactions on Power Electronics*, vol. 34, no. 8, pp. 7972–7982, 2019.

[12] R. Pintelon and J. Schoukens, *System Identification: A Frequency Domain Approach*. Wiley; IEEE Press, 2012.

[13] B. Bullecks, R. Suresh, and R. Rengaswamy, "Rapid impedance measurement using chirp signals for electrochemical system analysis," *Computers & chemical engineering*, vol. 106, pp. 421–436, 2017.

[14] C. Zhang, S. Føyen, J. Suul, and M. Molinas, "Modeling and analysis of sogi-pll/fll-based synchronization units: Stability impacts of different frequency-feedback paths," *IEEE Transactions on Energy Conversion*, vol. 36, no. 3, pp. 2047–2058, 2021.

[15] M. Colombino, D. Groß, and F. Dörfler, "Global phase and voltage synchronization for power inverters: A decentralized consensus-inspired approach," in *2017 IEEE 56th Annual Conference on Decision and Control (CDC)*, 2017, pp. 5690–5695.

[16] G. Seo, M. Colombino, I. Subotic, B. Johnson, D. Groß, and F. Dörfler, "Dispatchable virtual oscillator control for decentralized inverter-dominated power systems: Analysis and experiments," in *2019 IEEE Applied Power Electronics Conference and Exposition (APEC)*, 2019, pp. 561–566.

[17] C. Zhang, M. Molinas, S. Føyen, J. Suul, and T. Isobe, "An integrated method for generating vscs' periodical steady-state conditions and hss-based impedance model," *IEEE Transactions on Power Delivery*, vol. 35, no. 5, pp. 2544–2547, 2020.